



Gas release characteristics during carbonization of iron coke hot briquette and influence of heating rate

Zi-yu Wang^{1,2,3} · Dong Han^{1,2,3} · Zheng-gen Liu^{1,2,3} · Man-sheng Chu^{1,2,3} · Yong-jie Zhang¹ · Li-feng Zhang^{1,2,3} · Ji-wei Bao^{1,2,3} · Ming-yu Wang^{1,2,3}

Received: 17 August 2022 / Revised: 8 November 2022 / Accepted: 9 November 2022 / Published online: 26 July 2023
© China Iron and Steel Research Institute Group Co., Ltd. 2023

Abstract

The release characteristics of CH₄, H₂, CO and CO₂ from iron coke hot briquette (ICHB) during carbonization were studied. The results show that compared with briquette without iron ore, Fe₃O₄ can inhibit the release rate of H₂ and promote the production of CO and CO₂. In addition, when the heating rate increases from 3 to 7 °C/min, the release rates of CH₄ and H₂ increase, while the release rates of CO and CO₂ first increase and then decrease. The carbonization process of ICHB was segmented, and corresponding kinetic analysis was carried out. The results show that the activation energy of Stage II and Stage IV is higher in the carbonization process of ICHB, and the active pyrolysis of coal and the reduction of iron ore occur in these two stages. In addition, the effect of heating rate on the kinetic parameters of ICHB carbonization process was investigated. It was found that when the heating rate increased, the reaction activation energy of Stage IV decreased first and then increased, which was consistent with the release law of CO and CO₂. The analysis showed that the increase in heating rate leads to more reactions at higher temperatures, resulting in an increase in the release rate of some gases. In addition, thermal hysteresis can also cause some processes to fail to fully react at the end of heating. It is also found that the apparent activation energy and preexponential factor have kinetic compensation effect during the carbonization of ICHB.

Keywords Iron coke hot briquette · Carbonization · Gas release characteristic · Heating rate · Kinetics

1 Introduction

Recently, global warming has become a major concern for human beings, and this is mainly caused by the increase in CO₂ concentration in the atmosphere. CO₂ emissions from the iron and steel industry account for 5%–7% of the total carbon emissions [1, 2], which means that iron and steel enterprises will bear huge pressure of carbon emission

reduction. Modern steel production includes two main processes: integrated iron and steel plant and mini-mill. The pig iron production from blast furnace accounts for 70% of the total pig iron production, while the CO₂ emission from blast furnace ironmaking process accounts for 62% of the total iron production process [3]. Therefore, the low-carbon development of blast furnace production will be an important breakthrough to realize energy conservation and emission reduction in the iron and steel industry.

Ferro-coke is a kind of coke with high reactivity. The use of ferro-coke in blast furnace can reduce the temperature of thermal reserve zone and realize energy saving and emission reduction [4, 5]. When the temperature of thermal reserve zone decreases by 100 °C, the carbon consumption of blast furnace will decrease by 5%; if the temperature of thermal reserve zone reduces by 300 °C, the carbon consumption will decrease by 14% [6]. The preparation of ferro-coke mainly includes two processes: traditional coke

✉ Man-sheng Chu
chums@smm.neu.edu.cn

¹ School of Metallurgy, Northeastern University, Shenyang 110819, Liaoning, China

² Engineering Research Center of Frontier Technologies for Low-Carbon Steelmaking (Ministry of Education), Shenyang 110819, Liaoning, China

³ Liaoning Province Engineering Research Center for Technologies of Low-Carbon Steelmaking, Shenyang 110819, Liaoning, China

oven and shaft furnace with briquette as raw material. Using coke oven to produce ferro-coke can make full use of the existing equipment, but the iron ore reacts with refractory linings, especially silicon bricks, at 1200 °C to form fayalite, which causes the furnace wall to be damaged [7]. In another process, a mixture of iron ore and coal is heated to a certain temperature or a binder is added, and the mixture is made into briquette [8–13]. Then, the briquette was put into the shaft furnace for carbonization to get the iron coke product. Compared with coke oven, shaft furnace can effectively avoid the erosion of furnace wall and cannot use coke coal as raw material, effectively alleviating the shortage of high-quality coke coal resources. On October 9, 2020, JFE West Nippon Iron & Steel Co., Ltd. carried out a pilot test of the ferro-coke project. In the experiment, 30% iron ore and 70% pulverized coal were mixed as raw materials, and the ferro-coke was obtained by carbonization in a shaft furnace. The production capacity of this pilot plant can reach 300 t/d.

The shaft furnace has two heating intervals equipped with low-temperature tuyere and high-temperature tuyere, respectively. The role of the low-temperature tuyere is to reduce the heating rate of the briquette in the low-temperature range, so as to reduce the maximum thermal stress value of the briquette and suppress the generation of cracks. Bao et al. [14–17] studied the influence of carbonization process parameters on the mechanical strength, reactivity and post-reaction strength of ferro-coke. The results showed that under the optimized carbonization process conditions, the compressive strength of ferro-coke was greater than 3500 N, the reactivity was more than 60%, and the post-reaction strength was about 16%. Han et al. [18] analyzed the deformation mechanism of ferro-coke during carbonization and investigated the effects of heating rate, forming pressure and particle size of iron ore powder on the deformation behavior of ferro-coke. Xu et al. [19] studied the influence of iron ore type on thermal behavior and reaction kinetics in carbonization process by thermal analysis. Zhang et al. [20] prepared ferro-coke from different proportions of iron ore. The effect of iron ore on the microstructure of ferro-coke was studied, and the effect of the proportion of iron ore powder on the kinetic parameters of the gasification reaction of ferro-coke was investigated.

At present, there are few studies on the gas produced in the carbonization process of ferro-coke. The gas products of the carbonization process can be recovered as a high-quality fuel, which has many similarities in composition and properties with coke oven gas. On the other hand, the precipitation characteristics of gas products in the carbonization process also reflect the different stages of carbonization, which can be used as an effective method to detect the carbonization process. The characteristics of gas product precipitation in the carbonization process of ferro-

coke were studied in this paper. The influence of heating rate on the precipitation characteristics of gas products was investigated. At the same time, the changes of activation energy and preexponential factor in different stages of carbonization process at different heating rates were studied by piecewise kinetic calculation.

2 Experimental

2.1 Raw materials

One kind of iron ore and three kinds of coals were used to prepare iron coke hot briquette (ICHB). The chemical composition of iron ore sample is listed in Table 1. Iron ore A is a kind of magnetite with the total iron content of about 65.36% and the FeO content of about 21.86%. The proximate analysis and ultimate analysis of the coals are listed in Table 2. 90% of the iron ore and the coals has a size less than 150 μm and 80% is less than 75 μm .

2.2 Experimental procedures

The optimum raw material ratio of composite ferro-coke is 30% iron ore, 45% coal A, 20% coal B and 5% coal C [21]. The experimental results show that the compressive strength of the ferro-coke before and after carbonization can meet the needs of production, and it has good reactivity and strength after reaction. Iron ore and coal are mixed in proportion; the mixture is put into a mold, fed to an electric furnace, and heated to 300 °C. The mixture of heated iron ore and coal is kept at 50 MPa pressure for 1 min to get the hot briquette.

Two hundred gram hot briquettes were put into the tube of the vertical heating furnace shown in Fig. 1. Corundum balls with a diameter of 25 mm and a total height of 100–150 mm are padded under the sample to ensure that the heated sample is located in the constant-temperature section of the heating furnace. And when the gas enters the furnace tube, the corundum ball can play the role of rectification, so that the distribution of air flow is more uniform. The thermocouple is inserted into the sample to capture the sample temperature change at every moment. The furnace tube is connected to a weight-measuring ring at the bottom of the electronic balance by three hooks. The gas produced during the carbonization process is collected and sent to a gas analyzer. Thermocouples, electronic balances and gas analyzers are all connected to a computer. The computer captures the temperature, mass loss rate and gas composition of the sample at every moment during the carbonization process. Nitrogen with a flow rate of 5 L/min was continuously injected to protect the samples from oxidation during the carbonization process.

Table 1 Chemical composition of iron ore concentrate A (wt.%)

| TFe | FeO | CaO | SiO ₂ | MgO | Al ₂ O ₃ |
|-------|-------|------|------------------|------|--------------------------------|
| 65.36 | 21.86 | 0.17 | 6.35 | 0.45 | 0.45 |

Table 2 Proximate and ultimate analyses of coal samples (wt.%)

| Sample | Proximate analysis | | | | Ultimate analysis | | | | |
|------------|--------------------|-----------------|-----------------|------------------|-------------------|------|------|------|------|
| | M _{ad} | A _{ad} | V _{ad} | FC _{ad} | C | H | O | N | S |
| Coal 1 | 0.75 | 8.96 | 29.08 | 61.21 | 82.22 | 4.36 | 8.99 | 1.38 | 0.98 |
| Coal 2 | 0.44 | 9.90 | 13.16 | 76.50 | 86.00 | 4.11 | 4.42 | 1.19 | 0.93 |
| Coal 3 | 1.09 | 13.36 | 7.30 | 78.25 | 79.58 | 2.40 | 4.72 | 1.21 | 0.59 |
| Coal blend | 0.69 | 9.54 | 22.98 | 66.80 | 83.11 | 4.15 | 7.38 | 1.31 | 0.94 |

M_{ad}—Moisture in air dry basis; A_{ad}—ash in air dry basis; V_{ad}—volatile in air dry basis; FC_{ad}—fixed carbon in air dry basis

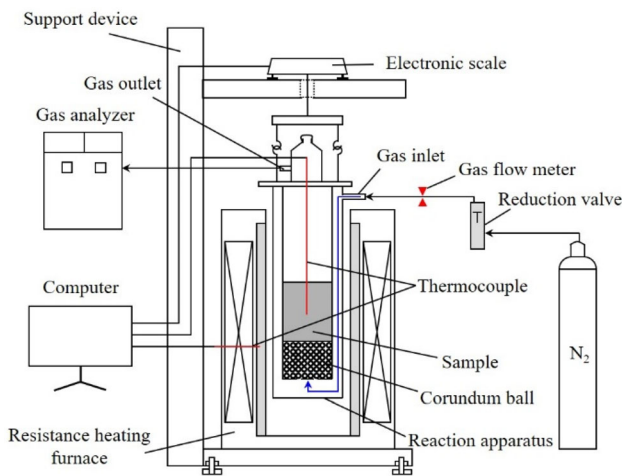


Fig. 1 Schematic diagram of ICHB carbonization equipment

The gas analyzer can record the composition of the precipitated gas at any time during the carbonization process, and the flow rate of a component in the gas product can be calculated according to Eqs. (1) and (2).

Total outlet gas flow is

$$Q_{out} = \frac{q_{N_2}}{C_{N_2}} \quad (1)$$

The flow rate of any gas component is

$$q_i = Q_{out} \times C_i \quad (2)$$

where Q_{out} is the total flow of gas from the carbonization unit, mmol/min; q_{N_2} is the flow rate of N₂ in the reaction process, mmol/min, which is considered as a constant before and after the reaction since N₂ does not react with ICHB during carbonization; C_{N_2} is the proportion of N₂ in the outlet gas, %; q_i is the flow rate of component i in the

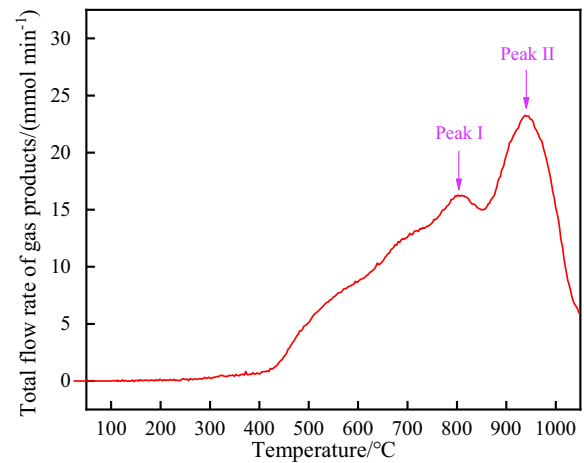


Fig. 2 Gas phase release rate during ICHB carbonization with heating rate of 3 °C/min

gas product of carbonization process, mmol/min; and C_i is the proportion of component i in the outlet gas, %.

3 Results and discussion

3.1 Characteristics of pyrolysis gas from ferro-coke during carbonization

The sample was raised from room temperature to 1050 °C at a heating rate of 3 °C/min. The precipitation rate of gas products during the carbonization of ICHB is shown in Fig. 2. Before 400 °C, the precipitation rate of pyrolysis gas was slow. When the temperature exceeds 400 °C, the precipitation rate of gas products increases rapidly with the increase in carbonization temperature. There are two peaks

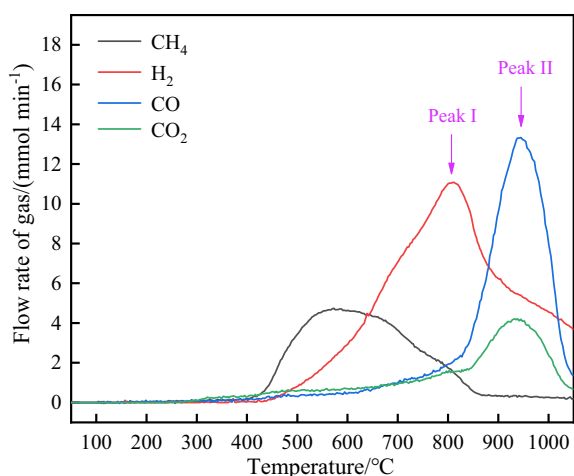


Fig. 3 Release rates of major gas components during carbonization of ICHB with heating rate of 3 °C/min

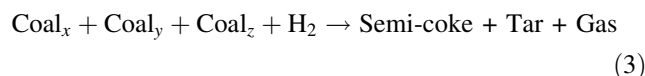
of pyrolysis gas release in the temperature range of 800–1000 °C. The first release peak (hereinafter referred to as Peak I) appears around 800 °C, and the release rate of gas is 16.29 mmol/min. The second release peak (hereinafter referred to as Peak II) occurs around 950 °C, and the gas release rate is 23.27 mmol/min. Subsequently, the release rate of gas products gradually decreases.

A gas analyzer was used to investigate the release rates of different components of gases during the carbonization of ICHB, and the results are shown in Fig. 3. CH₄ was released from around 400 °C. With the increase in the carbonization temperature, the release rate of CH₄ firstly increased and then decreased. The release rate of CH₄ reached the maximum at around 600 °C, and the maximum release rate was 4.74 mmol/min. H₂ also begins to be released around 400 °C. With the increase in the carbonization temperature, the release rate of H₂ first increased and then decreased. The release rate of H₂ reached the maximum at 800 °C, and the maximum release rate was 11.09 mmol/min. CO is slowly released from around 400 °C, and when the temperature rises to 800 °C, the release rate of CO increases rapidly. The release rate of CO reaches the maximum at around 950 °C, with the maximum release rate of 13.33 mmol/min, and then decreases rapidly. CO₂ releases slowly at around 400 °C, and the release rate increases rapidly when the temperature rises to 800 °C. The release rate reaches the maximum at around 950 °C, with a maximum release rate of 4.21 mmol/min, and then decreases rapidly. From the release of gas products, Peak I is formed due to the rapid release of H₂, and Peak II is formed due to the rapid release of CO and CO₂.

In general, CH₄ released during coal pyrolysis is mainly generated by aliphatic side chain breaking during coal pyrolysis. H₂ is mainly generated by the polycondensation

reaction in the process of coal pyrolysis, which changes from the aromatic ring with a smaller number of rings to the aromatic ring with a larger number of rings. This process is accompanied by the formation of hydrogen. The CO and CO₂ produced during coal pyrolysis mainly come from the decomposition of oxygen-containing functional groups such as the aromatic weak bonds and fat bonds [22]. However, the iron-containing component in the raw material has a certain influence on the volatile component release behavior in the process of carbonization, which is shown in the following aspects: iron-containing raw material has a certain catalytic effect on the pyrolysis process of coal; iron oxides in raw materials are reduced by reducing substances in coal to produce CO₂, which is further reduced to CO. In order to study the influence mechanism of iron and iron oxides on volatile component emission behavior in the process of pyrolysis, Al₂O₃ with the same mass fraction mixed with coal to prepare hot briquette in this study, which was marked as HBA. Al₂O₃ is equivalent to inert additives in the pyrolysis process of coal, which means that Al₂O₃ will not react with coal during the carbonization.

The HBA was heated to 1050 °C under the same conditions. The comparison of the release rates of each component of gas products during the carbonization of ICHB and HBA is shown in Fig. 4. As shown in Fig. 4a, b, the CH₄ release temperatures of ICHB and HBA are in the same range from 400 to 900 °C during carbonization, and the maximum release rate of CH₄ of HBA is higher. The H₂ release temperature of ICHB decreases slightly, but the H₂ release rate is significantly lower than that of HBA [23]. This result is mainly caused by magnetite in ICHB. The results show that Fe₃O₄ can effectively promote the formation of semi-coke during coal pyrolysis [24]. The pyrolysis process of coal includes not only the cracking of large molecules into small molecules of tar, gas and water, but also the polymerization of hydrogen and coal fragments into semi-coke.



As can be seen from Fig. 4c, d, the CO release law of ICHB and HBA gas products is similar with the increase in temperature before 700 °C. After 800 °C, the proportion of CO in HBA gas products begins to decrease, but the proportion of CO in ICHB gas products increases rapidly. This is because the Fe₃O₄ in iron ore around 800 °C began to be gradually reduced to metallic iron, and iron ore was tightly wrapped by coal. Under the condition of high temperature and excessive carbon, the reduction process of iron oxide can be expressed as Eqs. (4) and (5). This process is shown in Fig. 5. Iron oxides can catalyze the production of CO

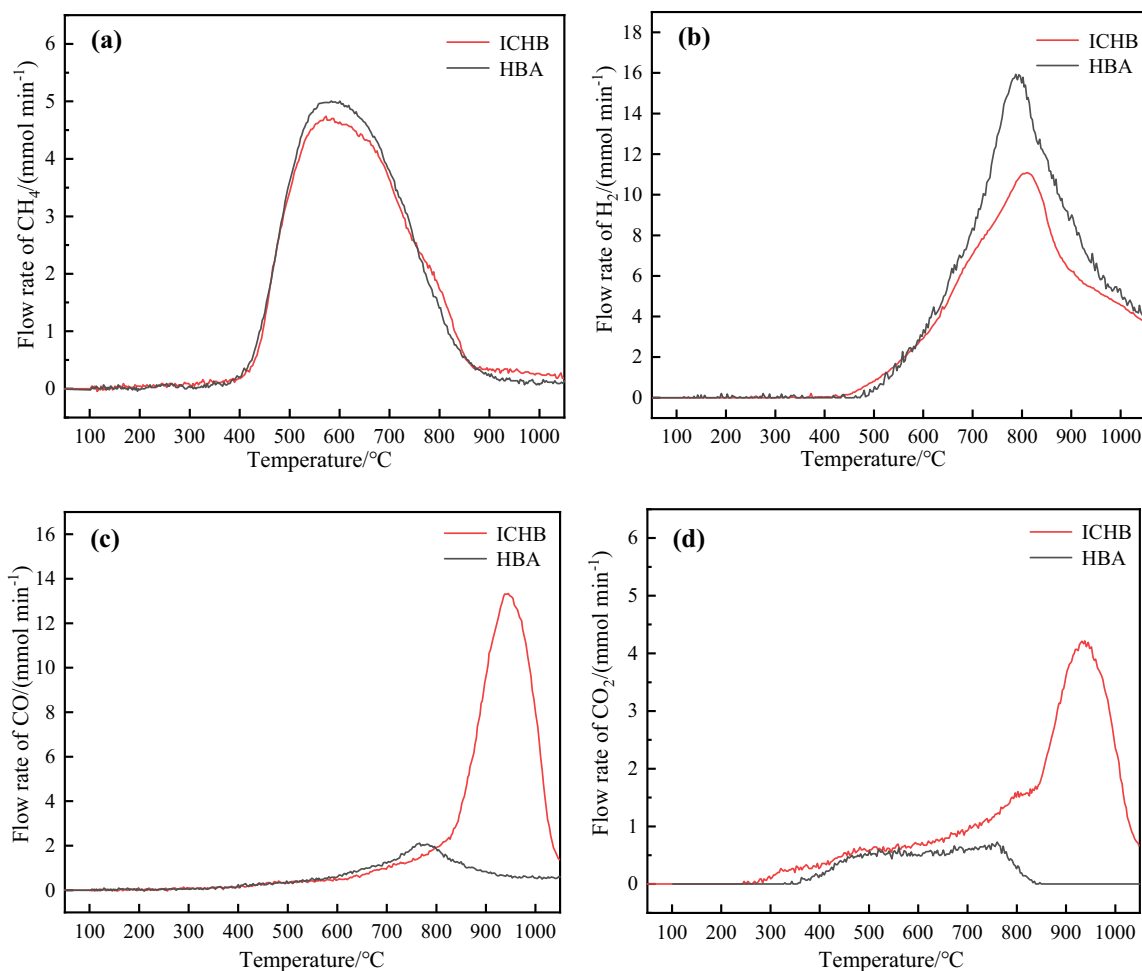


Fig. 4 Release rates of major gas components during carbonization of ICHB and HBA with heating rate of 3 °C/min. **a** CH₄; **b** H₂; **c** CO; **d** CO₂

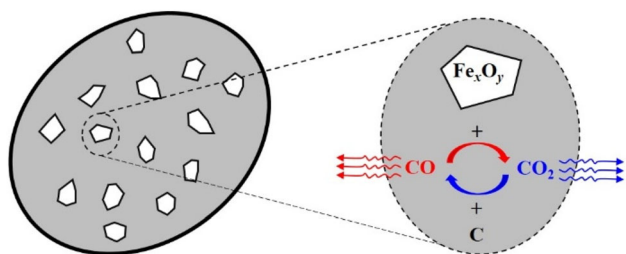
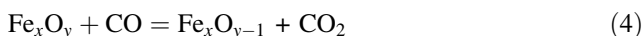


Fig. 5 Schematic diagram of coupling catalytic reaction between iron ore and coal

and CO₂ during coal pyrolysis. Fe_xO_y is reduced to a lower valence state, and the reduced CO₂ further reacts with the carbon in coal to form CO, which once again acts as a reducing agent to participate in the reduction process of iron ore. These two reactions promote each other and eventually lead to the increase in the ratio of CO and CO₂ in ICHB carbonization gas products.



3.2 Effect of heating rate on gas products of composite iron coking process and kinetic analysis

The samples were raised from room temperature to 1050 °C at the heating rates of 3, 5 and 7 °C/min, respectively, and the gas analyzer was used to investigate the precipitation rates of different components of gases in the carbonization process of ICHB at different heating rates, as shown in Fig. 6. It can be seen from Fig. 6a, b that with the increase in the heating rate, the temperature at which CH₄ reaches the maximum release rate increases, and the maximum release rate increases from 4.74 to 8.16 mmol/min. Similar to CH₄, with the increase in the heating rate, the temperature at which H₂ reaches the maximum release rate increases, and the maximum release rate increases from 11.09 to 18.42 mmol/min.

As can be seen from Fig. 6c, d, with the increase in the heating rate, the release process of CO and CO₂ shows a

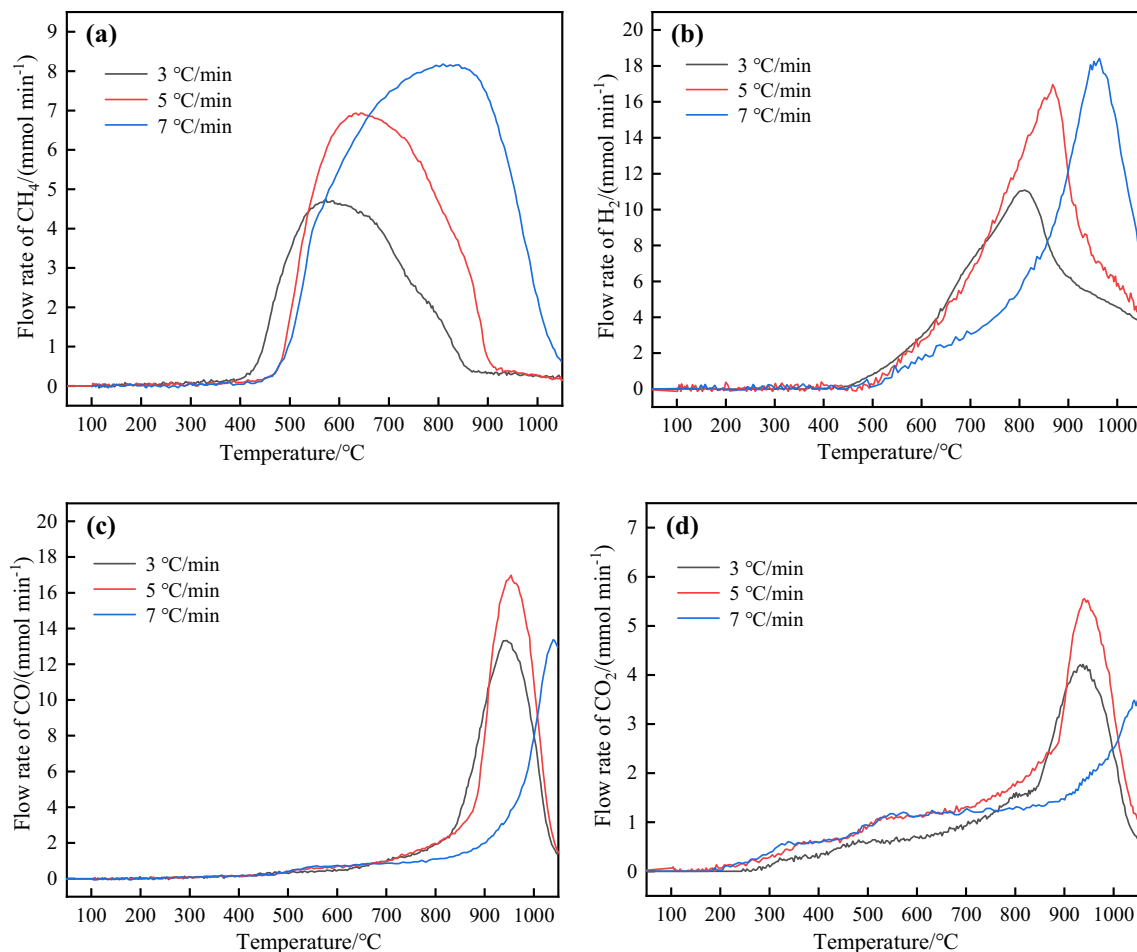


Fig. 6 Release rates of major gas components during carbonization of ICHB at different heating rates. **a** CH₄; **b** H₂; **c** CO; **d** CO₂

similar trend: when the heating rate increases from 3 to 5 °C/min, the temperature at which CO and CO₂ reach the maximum release rate almost does not change. However, the maximum release rates of CO and CO₂ increased to 16.98 and 5.55 mmol/min, respectively. When the heating rate increases to 7 °C/min, the temperature at which CO and CO₂ reach the maximum release rate increases, but the maximum release rate of CO and CO₂ decreases.

In general, temperature is the main factor affecting the pyrolysis reaction. When heated, the macromolecular compounds in coal decompose into aliphatic compounds, aromatic compounds, CH₄, H₂, CO and CO₂. However, increasing the heating rate will cause more of these reactions to occur at higher temperatures. It not only leads to the phenomenon of thermal delay in the release of gas products, but also promotes the release of gas products due to the increase in the reaction temperature.

In order to study the influence mechanism of heating rate on the pyrolysis process of ICHB, we analyzed the mass loss characteristics of ICHB at three different heating rates. And the thermogravimetric (TG) and differential

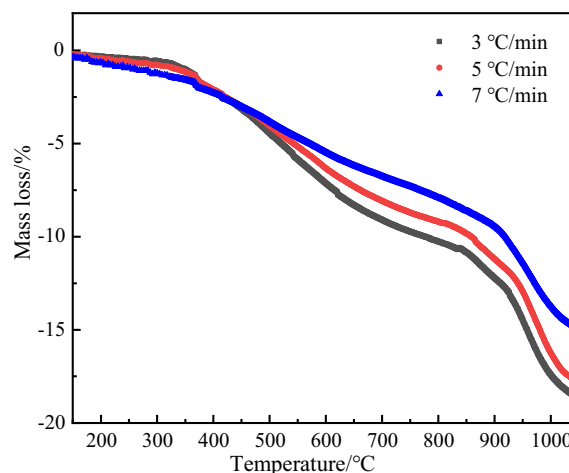


Fig. 7 Mass loss of ICHB during carbonization at different heating rates

thermogravimetric (DTG) curves are shown in Figs. 7 and 8. The mass loss rates of ICHB at the end of carbonization at three heating rates are 18.75%, 17.92% and 15.01%.

The conversion rate of ICHB in the carbonization process is shown in Eq. (6).

$$\alpha = \frac{w_0 - w_T}{w_0 - w_f} \times 100\% \tag{6}$$

where α is the conversion rate, %; w_0 is the initial mass of ICHB sample, g; w_T is the mass of ICHB sample at temperature T , g; and w_f is the mass of ICHB at the end of carbonization, g.

The reaction rate is shown in Eq. (7).

$$\frac{d\alpha}{dt} = k(T) \cdot f(\alpha) \tag{7}$$

where t is the carbonization time, min; $k(T)$ is the rate constant; and $f(\alpha)$ is the differential form of the reaction mechanism function. $k(T)$ is calculated by the Arrhenius equation, as shown in Eq. (8).

$$k(T) = A \exp\left(-\frac{E}{RT}\right) \tag{8}$$

where A is the preexponential factor, s^{-1} ; E is the activation energy, kJ/mol; and R is the gas constant, J/(mol K).

Under non-isothermal test conditions, the heating rate β is a constant and can be obtained according to $\beta = dT/dt$.

$$\frac{d\alpha}{f(\alpha)} = \frac{1}{\beta} A \exp\left(-\frac{E}{RT}\right) dT \tag{9}$$

Equation (9) is integrated, and the result is shown in Eq. (10).

$$\int_0^\alpha \frac{d\alpha}{f(\alpha)} = G(\alpha) = \frac{A}{\beta} \int_{T_0}^T \exp\left(-\frac{E}{RT}\right) dT \tag{10}$$

where T_0 is the initial temperature of ICHB sample.

The Coats-Redfern (CR) integral method is applied to Eq. (10), and the result is shown in Eq. (11).

$$\ln\left(\frac{G(\alpha)}{T^2}\right) = \ln\left[\frac{AR}{\beta E}\right] - \frac{E}{RT} \tag{11}$$

According to Eq. (11), $\ln(G(\alpha)/T^2)$ and T^{-1} have a linear relationship in theory, where the slope of the line is $(-E/R)$ and the vertical intercept is $\ln[(AR)/(\beta E)]$. Thus, the activation energy and preexponential factor of the reaction can be obtained. If the theoretical curve fits well with the test curve, the mechanism function represented by the theoretical curve is the most probable mechanism function. Common mechanism functions [25–27] used to describe gas–solid reactions are shown in Table 3.

According to the DTG curve, the carbonization process of ICHB from 200 to 1000 °C can be divided into four stages, as shown in Table 4. Before 200 °C, the removal of water is the main process. Since this process is hardly affected by the heating rate, the reaction at this stage is not considered in this study. The calculation results of kinetic parameters of ICHB carbonization at a heating rate of 3 °C/min are shown in Table 4.

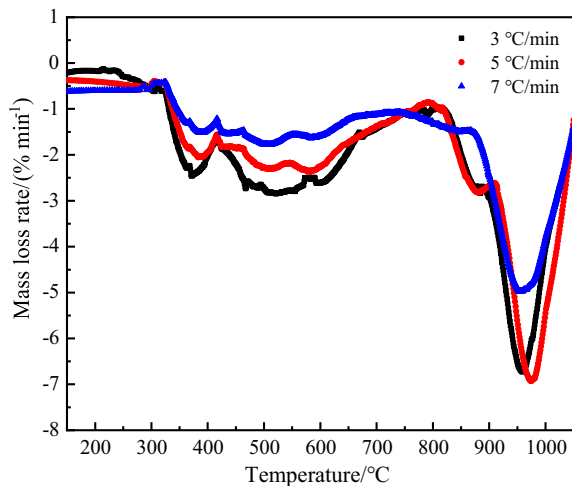


Fig. 8 Mass loss rate of ICHB during carbonization at different heating rates

Table 3 Common mechanism functions describing gas–solid reactions

| Code | Mechanism | $f(\alpha)$ | $G(\alpha)$ |
|----------------|---|--|--|
| F ₁ | Chemical reaction ($n = 1$) | $(1 - \alpha)$ | $-\ln(1 - \alpha)$ |
| F ₂ | Chemical reaction ($n = 2$) | $(1 - \alpha)^2$ | $(1 - \alpha)^{-1} - 1$ |
| F ₃ | Chemical reaction ($n = 3$) | $(1 - \alpha)^3$ | $[(1 - \alpha)^{-2} - 1]/2$ |
| A ₂ | Random nucleation and nuclei growth (two-dimensional) | $2(1 - \alpha)[- \ln(1 - \alpha)]^{1/2}$ | $[- \ln(1 - \alpha)]^{1/2}$ |
| A ₃ | Random nucleation and nuclei growth (three-dimensional) | $3(1 - \alpha)[- \ln(1 - \alpha)]^{2/3}$ | $[- \ln(1 - \alpha)]^{2/3}$ |
| R ₂ | Shrinking core (cylinder) | $2(1 - \alpha)^{1/2}$ | $1 - (1 - \alpha)^{1/2}$ |
| R ₃ | Shrinking core (sphere) | $3(1 - \alpha)^{2/3}$ | $1 - (1 - \alpha)^{1/3}$ |
| D ₁ | One-dimensional diffusion control | $(1/2)\alpha$ | α^2 |
| D ₂ | Two-dimensional diffusion control | $[- \ln(1 - \alpha)]^{-1}$ | $\alpha + (1 - \alpha)\ln(1 - \alpha)$ |
| D ₃ | Three-dimensional diffusion control | $(3/2)[(1 - \alpha)^{1/3} - 1]^{-1}$ | $(1 - 2\alpha/3) - (1 - \alpha)^{2/3}$ |

n —Order of reaction

Table 4 Kinetic parameters of ICHB using different mechanism functions with heating rate of 3 °C/min

| Code | Stage I (200–320 °C) | | Stage II (320–420 °C) | | Stage III (420–820 °C) | | Stage IV (820–1000 °C) | |
|----------------|----------------------|------------------------|-----------------------|-----------------------|------------------------|------------------------|------------------------|-----------------------|
| | $E/(kJ\ mol^{-1})$ | A/s^{-1} | $E/(kJ\ mol^{-1})$ | A/s^{-1} | $E/(kJ\ mol^{-1})$ | A/s^{-1} | $E/(kJ\ mol^{-1})$ | A/s^{-1} |
| F ₁ | 3.92 | 4.65×10^{-7} | 41.35 | 9.94×10^{-3} | 13.05 | 2.47×10^{-5} | 53.71 | 6.15×10^{-3} |
| F ₂ | 4.08 | 5.09×10^{-7} | 43.51 | 1.64×10^{-2} | 19.29 | 1.11×10^{-4} | 116.22 | 15.92 |
| F ₃ | 4.24 | 5.57×10^{-7} | 45.73 | 2.72×10^{-2} | 26.43 | 5.40×10^{-4} | 197.82 | 2.60×10^5 |
| A ₂ | -2.46 | -4.36×10^{-7} | 15.32 | 1.01×10^{-4} | -0.72 | -3.08×10^{-7} | 17.04 | 4.23×10^{-5} |
| A ₃ | -0.33 | -5.15×10^{-8} | 23.99 | 5.25×10^{-4} | 3.87 | 2.72×10^{-6} | 29.26 | 2.60×10^{-4} |
| R ₂ | 3.84 | 2.22×10^{-7} | 40.29 | 3.89×10^{-3} | 10.27 | 5.87×10^{-6} | 31.56 | 1.40×10^{-4} |
| R ₃ | 3.86 | 1.51×10^{-7} | 40.64 | 2.81×10^{-3} | 11.17 | 5.01×10^{-6} | 38.27 | 2.46×10^{-4} |
| D ₁ | 16.35 | 7.88×10^{-7} | 89.23 | 11.97 | 29.93 | 1.59×10^{-4} | 50.07 | 1.54×10^{-3} |
| D ₂ | 16.45 | 4.10×10^{-7} | 90.60 | 8.09 | 33.19 | 1.60×10^{-4} | 68.81 | 9.93×10^{-3} |
| D ₃ | 16.49 | 9.22×10^{-8} | 91.07 | 1.99 | 34.40 | 4.58×10^{-5} | 77.70 | 7.02×10^{-3} |

R^2 —Determination coefficient

Table 5 Kinetic parameters of ICHB at different heating rates

| Stage | Heating rate/(°C min ⁻¹) | Temperature range/°C | $E/(kJ\ mol^{-1})$ | A/s^{-1} |
|-------|--------------------------------------|----------------------|--------------------|-----------------------|
| I | 3 | 200–320 | 16.49 | 9.22×10^{-8} |
| | 5 | 200–320 | 18.13 | 2.98×10^{-7} |
| | 7 | 200–320 | 18.97 | 1.34×10^{-6} |
| II | 3 | 320–420 | 91.07 | 1.99 |
| | 5 | 320–420 | 68.79 | 2.83×10^{-2} |
| | 7 | 320–420 | 36.62 | 8.36×10^{-5} |
| III | 3 | 420–820 | 34.40 | 4.58×10^{-5} |
| | 5 | 420–800 | 32.76 | 3.09×10^{-5} |
| | 7 | 420–860 | 24.10 | 7.72×10^{-6} |
| IV | 3 | 820–1000 | 77.70 | 7.02×10^{-3} |
| | 5 | 800–1000 | 67.57 | 1.93×10^{-3} |
| | 7 | 860–1000 | 97.74 | 5.96×10^{-2} |

The fitting results show that the D₃ model has the best linear relationship with 1/T in each stage of ICHB carbonization, which means that there is the possibility of diffusion control mechanism in ICHB carbonization stage. The kinetic parameters of ICHB carbonization at heating rates of 3, 5 and 7 °C/min were obtained by fitting the D₃ model as shown in Table 5. Stage I is the soft melting process of coal, accompanied by the fracture of weak bonds and active functional groups in the coal molecular structure. The energy required for this process is relatively low, so that the apparent activation energy of the reaction is also low. In order to avoid cracking of ferro-coke affecting mechanical strength during carbonization, the heating rate of ICHB during carbonization is generally controlled at a relatively low level in actual production [28]. At a lower heating rate, the activation energy of the Stage I reaction increases with the increase in the heating rate, which has the same property as the pyrolysis process of coal [29, 30]. Stage II of ICHB carbonization belongs to the active decomposition stage. At this time, depolymerization and decomposition of coal occur, and the reaction needs to consume a large amount of energy. Therefore, the apparent activation energy at this stage is high, and the increase in heating rate can reduce the activation energy required for this reaction process. Secondary pyrolysis of semi-coke occurs in Stage III on the basis of Stage II, which requires less energy than Stage II. At the same time, a higher heating rate can also reduce the activation energy required for this stage of the reaction. Stage IV is unique to the carbonization process of ICHB, and the reduction process of iron ore mainly occurs in this stage. The composition of iron ore used in this study is Fe₃O₄; thus, its reduction process occurs at a higher temperature. As can be seen from Table 5, with the increase in the heating rate, the activation energy of the reaction at this stage decreases

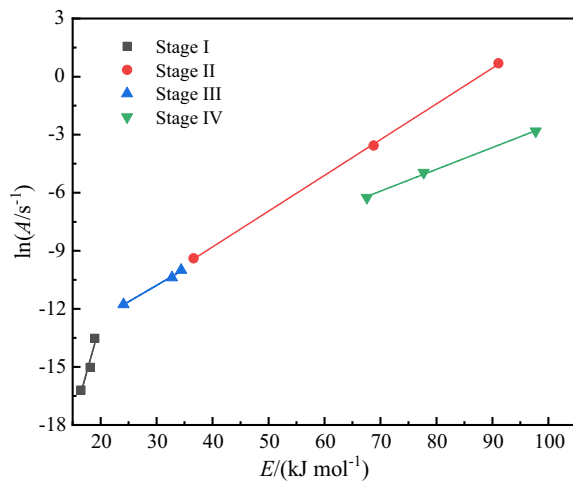


Fig. 9 Relationship between $\ln A$ and E of ICHB with different stages

first and then increases. This indicates that the increase in the heating rate can promote the reduction of iron ore. However, an increase in the heating rate also causes a thermal delay in the reaction, meaning that the temperature at which the reaction starts and ends becomes higher. This also leads to an increase in the activation energy of the reaction when the heating rate is too high. This conclusion is also consistent with the precipitation characteristics of gas products during carbonization.

Taking the activation energy of the reaction at different stages as the abscissa and the logarithm of the preexponential factor as the ordinate, the relationship between $\ln A$ and E is obtained, as shown in Fig. 9. In the four stages of ICHB carbonization, the linear correlation between activation energy and $\ln A$ is: 0.8712, 0.9996, 0.9920 and 0.9959, respectively. The fitting results are good, which means that there is a good linear compensation effect between activation energy and preexponential factor in the carbonization process of ICHB.

4 Conclusions

1. Compared with briquette without iron ore, the H_2 release rate of ICHB during carbonization is reduced, which is related to the promoting effect of Fe_3O_4 on the formation of semi-coke. The release rate of CO and CO_2 increases, which is closely related to the reduction of iron ore at high temperature.
2. The heating rate affects the precipitation characteristics of gas products during the carbonization of ICHB. With the increase in the heating rate, the release rate of CH_4 and H_2 increases, while the release rate of CO and CO_2 first increases and then decreases. According to the analysis of the release curve and the activation

energy of gas products, the increase in heating rate leads to more reactions at higher temperatures. This results in an increase in the release rate of some gases, such as CH_4 and H_2 . In addition, thermal hysteresis can also cause some processes to fail to fully react at the end of heating.

3. The mass loss curves of ICHB under different heating rates were compared. When the heating rate is 3, 5, and 7 °C/min, the mass loss rate of ICHB at the end of carbonization is 18.75%, 17.92%, and 15.01%, respectively.
4. By analyzing the TG and DTG curves of ICHB at different heating rates, the carbonization process of ICHB can be divided into four stages from 200 to 1000 °C. The activation energy of Stage II is higher than those of Stage I and Stage III. At this time, depolymerization and decomposition of coal consume a lot of energy. The activation energy of Stage IV is also relatively high, and the reduction of iron ore is the main reaction at this time.
5. There is a good linear compensation effect between activation energy and preexponential factor in the carbonization process of ICHB.

Acknowledgements This work was financially supported by the National Natural Science Foundation of China-Liaoning Joint Funds (U1808212), National Natural Science Foundation of China (52074080) and Xingliao Talent Plan (XLYC1902118).

Declarations

Conflict of interest The authors declare that they have no conflict of interest.

References

- [1] X. Xing, H. Rogers, G.Q. Zhang, K. Hockings, P. Zulli, A. Deev, J. Mathieson, O. Ostrovski, *Fuel Process. Technol.* 157 (2017) 42–51.
- [2] H.T. Wang, W. Zhao, M.S. Chu, Z.G. Liu, J. Tang, Z.W. Ying, *Powder Technol.* 328 (2018) 318–328.
- [3] M.M. Sun, X.J. Ning, J.L. Zhang, K.J. Li, G.W. Wang, H.Y. Wang, *China Metallurgy* 28 (2018) No. 3, 1–8.
- [4] J. Guo, M.S. Chu, J. Tang, F. Li, Z.G. Liu, J.W. Bao, *Iron and Steel* 57 (2022) No. 8, 30–38.
- [5] C. Yin, M.X. Song, S.F. Zhang, in: *Minerals Metals & Materials Series: 12th International Symposium on High-Temperature Metallurgical Processing*, Anaheim, CA, USA, 2022, pp. 351–362.
- [6] Y. Ujisawa, K. Nakano, Y. Matsukura, K. Sunahara, S. Komatsu, T. Yamamoto, *ISIJ Int.* 45 (2005) 1379–1385.
- [7] S. Nomura, H. Terashima, E. Sato, M. Naito, *ISIJ Int.* 47 (2007) 823–830.
- [8] H.T. Wang, M.S. Chu, B.Y. Guo, J.W. Bao, W. Zhao, Z.G. Liu, J. Tang, *Steel Res. Int.* 90 (2019) 1800354.
- [9] H.T. Wang, M.S. Chu, J.W. Bao, Z.G. Liu, H.M. Long, *J. Iron Steel Res. Int.* 29 (2022) 741–750.

- [10] H.T. Wang, M.S. Chu, J.W. Bao, Z.G. Liu, J. Tang, H.M. Long, *Fuel* 268 (2020) 117339.
- [11] H.T. Wang, M.S. Chu, W. Zhao, Z.G. Liu, J. Tang, *Metall. Mater. Trans. B* 50 (2019) 324–336.
- [12] H.T. Wang, M.S. Chu, Z.H. Wang, W. Zhao, Z.G. Liu, J. Tang, Z.W. Ying, *JOM* 70 (2018) 1929–1936.
- [13] S.X. Qiu, S.F. Zhang, Q.Y. Zhang, G.B. Qiu, L.Y. Wen, *J. Iron Steel Res. Int.* 24 (2017) 1169–1176.
- [14] J.W. Bao, M.S. Chu, Z.G. Liu, D. Han, L.G. Cao, J. Guo, *J. Iron Steel Res.* 32 (2020) 532–541.
- [15] J.W. Bao, M.S. Chu, Z.G. Liu, D. Han, J. Guo, L.F. Zhang, *Steel Res. Int.* 93 (2022) 2100345.
- [16] J.W. Bao, M.S. Chu, Z.G. Liu, W. Lv, J. Guo, L.F. Zhang, *Ironmak. Steelmak.* 49 (2022) 239–254.
- [17] J.W. Bao, Z.G. Liu, M.S. Chu, D. Han, L.G. Cao, J. Guo, Z.C. Zhao, *Int. J. Miner. Metall. Mater.* 28 (2021) 1917–1928.
- [18] D. Han, Z.G. Liu, M.S. Chu, Y.J. Zhang, J.W. Bao, M.Y. Wang, L.G. Cao, *Metall. Mater. Trans. B* 53 (2022) 1631–1643.
- [19] R.S. Xu, B.W. Dai, W. Wang, J. Schenk, Z.L. Xue, *Fuel Process. Technol.* 173 (2018) 11–20.
- [20] J.L. Zhang, J. Guo, G.W. Wang, L.M. Zhang, T. Xu, C.L. Zheng, *Iron and Steel* 51 (2016) No. 9, 22–29.
- [21] J.W. Bao, M.S. Chu, H.T. Wang, Z.G. Liu, D. Han, L.G. Cao, J. Guo, Z.C. Zhao, *Metall. Mater. Trans. B* 51 (2020) 2785–2796.
- [22] L.H. Zhao, H.Q. Guo, Q.L. Ma, *Coal Conversion* 30 (2007) No. 1, 5–9.
- [23] R. Cypres, C. Soudan-Moinet, *Fuel* 59 (1980) 48–54.
- [24] X.F. Zheng, A.N. Zhou, X.X. Yang, *Guangzhou Chemical Industry* 44 (2016) No. 5, 100–102+105.
- [25] L.T. Vlaev, I.G. Markovska, L.A. Lyubchev, *Thermochim. Acta* 406 (2003) 1–7.
- [26] S.P. Zou, Y.L. Wu, M.D. Yang, J.A. Zhang, C. Li, J.M. Tong, *J. Commodity Sci. Technol. Quality* 13 (2007) No. 4, 330–334.
- [27] S.F. Zhang, F. Zhu, C.G. Bai, L.Y. Wen, H.J. Peng, *Ironmak. Steelmak.* 41 (2014) 219–228.
- [28] T. Anyashiki, H. Fujimoto, T. Yamamoto, T. Sato, H. Matsuno, M. Sato, K. Takeda, *Tetsu-to-Hagané* 101 (2015) 515–523.
- [29] J.H. Wang, L.P. Chang, K.C. Xie, *Coal Conversion* 32 (2009) No. 3, 1–5.
- [30] L. Chang, *Coal Processing and Comprehensive Utilization* (2021) No. 6, 59–64.

Springer Nature or its licensor (e.g. a society or other partner) holds exclusive rights to this article under a publishing agreement with the author(s) or other rightsholder(s); author self-archiving of the accepted manuscript version of this article is solely governed by the terms of such publishing agreement and applicable law.